Geochemistry Geophysics Geosystems G3

Article
Volume 14, Number 1
28 January 2013
doi:10.1029/2012GC004424
ISSN: 1525-2027

Published by AGU and the Geochemical Society

Effects of lithospheric viscoelastic relaxation on the contemporary deformation following the 1959 M_w 7.3 Hebgen Lake, Montana, earthquake and other areas of the intermountain seismic belt

Wu-Lung Chang
Department of Earth Sciences, National Central University, Chungli, Taiwan (wuchang@ncu.edu.tw)

Robert B. Smith
Department of Geology and Geophysics, University of Utah, Salt Lake City, Utah, USA

Christine M. Puskas
UNAVCO, Boulder, Colorado, USA

[1] The 1959 M_w 7.3 Hebgen Lake, MT, normal-faulting earthquake occurred in an extensional stress regime near the Yellowstone volcanic field. Time-dependent crustal deformation data following this major earthquake were acquired by precise trilateration and GPS surveys from 1973 to 2000 around the Hebgen Lake fault zone. Modeling the changes of baseline lengths across and near the fault reveals a lateral variation of transient rheology, in which the lithosphere is stronger near the Hebgen Lake fault zone than in the vicinity of the Yellowstone volcano system. The models also imply that the lower crust is stronger than the upper mantle, in agreement with results from studies of postseismic and post-lake-filling relaxations (<~100 years). In addition, evaluations of the postseismic motion produced by the Hebgen Lake and the 1983 M_w 6.9 Borah Peak, ID, earthquakes indicate that horizontal transient motion of up to ~1 mm/yr contribute significantly to the contemporary regional crustal deformation near the epicentral areas. For the eastern Basin and Range, ~500 km south of the Hebgen Lake fault, similar rheologic models were derived from the observed uplift associated with the Lake Bonneville rebound and were used to evaluate the postseismic deformation associated with six most recent paleoearthquakes of the Wasatch fault zone and three $M \geq 5.6$ historic earthquakes of northern Utah. The results show ≤0.1 mm/yr of horizontal postseismic motion at present time that are within the horizontal uncertainties of continuous GPS velocity from the Basin and Range and significantly smaller than the contemporary extension of 1–3 mm/yr in the Wasatch Front.

Components: 8,700 words, 11 figures, 1 table.

Index Terms: 1207 Geodesy and Gravity: Transient deformation (6924, 7230, 7240); 1236 Geodesy and Gravity: Rheology of the lithosphere and mantle (7218, 8160); 1240 Geodesy and Gravity: Satellite geodesy: results (6929, 7215, 7230, 7240).

Received 6 September 2012; **Revised** 9 November 2012; **Accepted** 15 November 2012; **Published** 28 January 2013.

Chang, W.L., R. B. Smith, and C. M. Puskas (2013), Effects of lithospheric viscoelastic relaxation on the contemporary deformation following the 1959 M_w 7.3 Hebgen Lake, Montana, earthquake and other areas of the intermountain seismic belt, *Geochem. Geophys. Geosyst.*, *14*, 1–17, doi:10.1029/2012GC004424.

1. Introduction

[2] The effects of viscoelastic loading and relaxation of the Earth's lithosphere are key elements in post- and interseismic stress associated with the earthquake cycle. An earthquake is assumed to generate coseismic stresses in a ductile lower crust and upper mantle, where materials are too weak to sustain long-term shear stresses. The shear stresses are however released over decades following an earthquake. Strains caused by the postseismic stress relaxation are in turn transferred through the elastic upper crust, producing observable transient deformation on the surface [e.g., *Thatcher*, 1983; *Pollitz*, 2003a; *Freed and Bürgmann*, 2004; *Gourmelen and Amelung*, 2005].

[3] The 1959 M_w 7.3 Hebgen Lake, MT, earthquake, the largest historic normal-faulting earthquake of the Intermountain Seismic Belt [*Smith and Sbar*, 1974], was located ~10 km northwest of the Yellowstone volcanic system (Figure 1). The earthquake ruptured 38 km along two segments of the Hebgen Lake fault zone with up to 6.1 m of surface displacement [*Doser*, 1985; *Barrientos et al*., 1987]. *Reilinger et al*. [1977] first observed a crustal uplift rate of 3–5 mm/yr following the earthquake by precise leveling surveys from 1923 to 1960 surrounding the epicenter and aftershock area of the Hebgen Lake earthquake. Further leveling measurements up to 1983 revealed that this rate appeared to have decreased exponentially with a characteristic decay time of about 10 years, suggesting a rheologic model with a 30–40 km thick elastic layer overlying a viscoelastic half-space with a viscosity of ~10^{19} Pa-s [*Reilinger*, 1986]. *Nishimura and Thatcher* [2003, 2004] further developed a similar model based on leveling data acquired in 1959–1987 around the Hebgen Lake fault, with 38 ± 8 km for elastic thickness and $4 \times 10^{18\pm0.5}$ Pa-s for half-space viscosity.

[4] In this study, we investigated the lithospheric rheology beneath the Hebgen Lake fault zone using deformation data obtained by trilateration and GPS surveys between 1973 and 2000 [*Savage et al*., 1993; *Puskas et al*., 2007], a period of 14–41 years after the earthquake. The Hebgen Lake GPS and trilateration baselines cross the fault at its largest offset as well as the aftershock zone on the northwest side of the Yellowstone Plateau (Figure 2). Time-dependent changes of baseline lengths were used to assess two-layer rheologic models: an elastic layer above a viscoelastic layer and half-space that corresponds to the upper crust, lower crust, and upper mantle of the lithosphere, respectively.

[5] We then assessed the postseismic viscoelastic effects to the contemporary crustal deformation in two extensional stress regimes of the Intermountain Seismic Belt. The combined postseismic deformation of the Hebgen Lake and the M_w 6.9 1983 Borah Peak, ID, earthquakes north of the Snake River Plain was first evaluated. In the Wasatch fault zone, UT, ~500 km to the south of the Hebgen Lake fault and on the east edge of the Basin and Range, postseismic deformation was also modeled for the six most recent Holocene paleoearthquakes and three large ($M > 5.6$) historic earthquakes of northern Utah. Comparing these results with the horizontal ground motion measured by GPS reveals how postseismic signals contribute to the contemporary regional deformation, and can thus affect notably (Snake River Plain) or insignificantly (Wasatch) to the determination of intraplate kinematic models.

2. Seismic and Crustal Deformation Observations

[6] The Hebgen Lake earthquake occurred in the northern Intermountain Seismic Belt near the Yellowstone volcanic area. A catalog of relocated earthquakes (1973–2011) of the Yellowstone-Hebgen Lake area, from a three-dimensional tomographically determined velocity model [*Husen and Smith*, 2004; *Farrell et al*., 2009], provided precise hypocenter information of the Yellowstone volcanic field and the southeast end of the Hebgen Lake fault zone. Figure 2 shows that the 90th-percentile distribution of focal depths, proposed to be a good estimate of the brittle-ductile transition [*Smith and Bruhn*, 1984], increases notably westward. This trend marks a systematic increase of the depths from ~5 km at the Yellowstone caldera to ~10–15 km at the Hebgen Lake fault zone, and further coincides with a significant decrease of thermal gradient in the crust from 70 °C/km to 25 °C/km [*Smith and Braile*, 1994].

[7] Trilateration and GPS techniques have been implemented to determine the three-dimensional deformation field of the Hebgen Lake area (Figure 1). The U.S. Geological Survey conducted seven trilateration surveys from 1973 to 1987 in the Hebgen Lake area, measuring the distances between 10 geodetic monuments with Geodolite, a precise laser-based EDM (electro-optical distance measure) instrument [*Savage et al*., 1993]. The data yield a uniaxial extensional strain rate of 0.266 ± 0.014 μstrain/yr across the Hebgen Lake fault, with an orientation of N15°E ± 1° that is nearly orthogonal to the

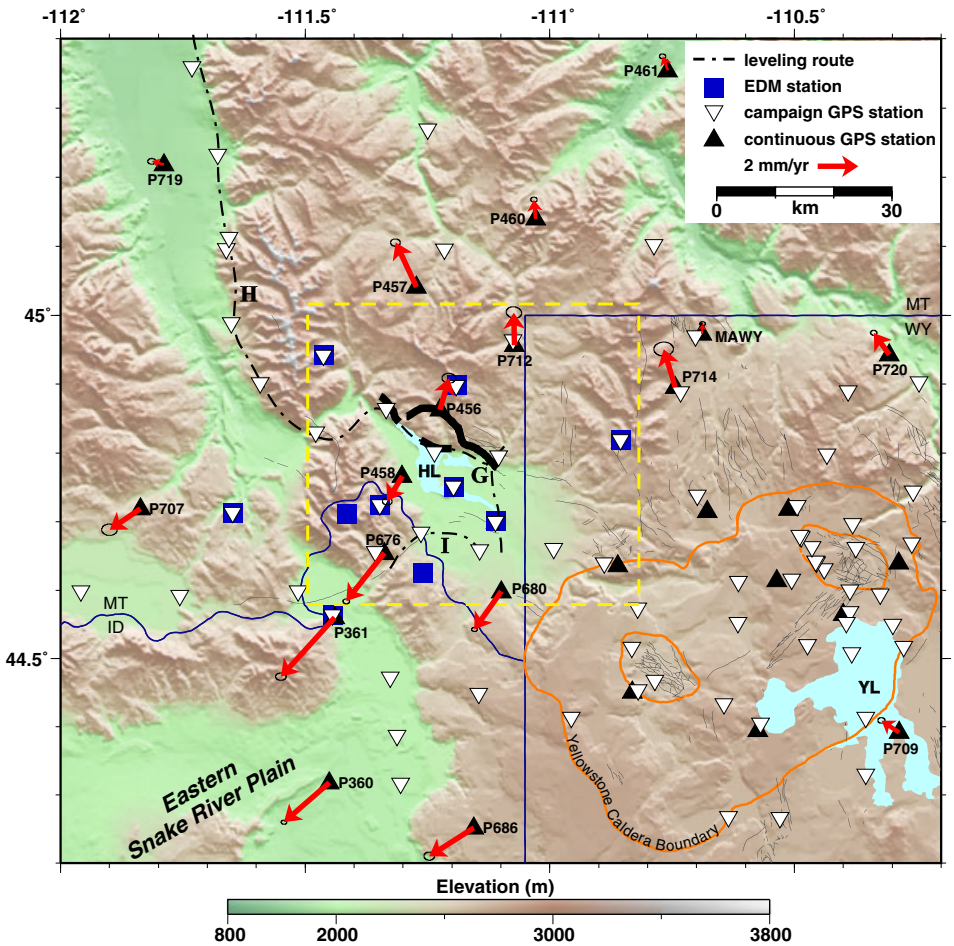

Figure 1. Topographic map and geodetic network of the Yellowstone-Hebgen Lake study area. Dot-dashed lines G, H, and I show leveling routes examined in this study (Figure 8). Thick black lines mark the surface ruptures of the 1959 M_w 7.3 Hebgen Lake, MT, earthquake. Orange line represents the boundary of the youngest Yellowstone caldera formed 0.65 Ma. Red arrows with 2-σ error ellipses show 2005–2011 horizontal velocities of continuous GPS sites (excluding those inside the Yellowstone caldera). Yellow dashed box corresponds to the study area shown in Figure 3. HL, Hebgen Lake; YL, Yellowstone Lake.

strike of the fault. This strain rate corresponds to a displacement rate of ~10.6 mm/yr across the 40 km aperture of the trilateration network.

[8] The University of Utah conducted GPS campaigns in 1987, 1989, 1991, 1993, 1995, and 2000 in an area covering a 200 km wide zone of Yellowstone and the adjacent eastern Snake River Plain to supplement the earlier geodetic surveys [*Puskas*, 2000, *Puskas et al.*, 2007]. These campaigns surveyed 140 sites of which 16 provide baselines that span in the ~50 km aperture of the Hebgen Lake fault zone (Figure 1). For each survey, the GPS receivers were programmed to record a minimum of two sessions of at least 8 h each. The 1987 and 1989 sessions were a shorter 6–7 h, due to limited satellite visibility in the early period of GPS technology. Data in a session were recorded at 30 s sampling intervals.

[9] In addition to the campaign GPS surveys, the University of Utah and the Plate Boundary Observatory have operated 10 continuous-recording GPS stations in northwest Yellowstone since 2005 to monitor ground movement across the Hebgen Lake fault zone. Figure 1 shows the locations of these stations along with their average horizontal velocities from 2005 to 2011 in a stable North American reference frame [*Chang et al.*, 2006]. In this study, we excluded GPS observations inside the Yellowstone caldera, where ground motions of these sites have been notably affected by the 2004–2010 episode of accelerated caldera uplift [*Chang et al.*, 2010].

[10] The campaign and continuous GPS data were processed with Bernese 4.2 processing software [*Hugentobler et al.*, 2001]. Precise orbits from the International GNSS Service were used for campaigns from 1995 onwards. For earlier campaign surveys,

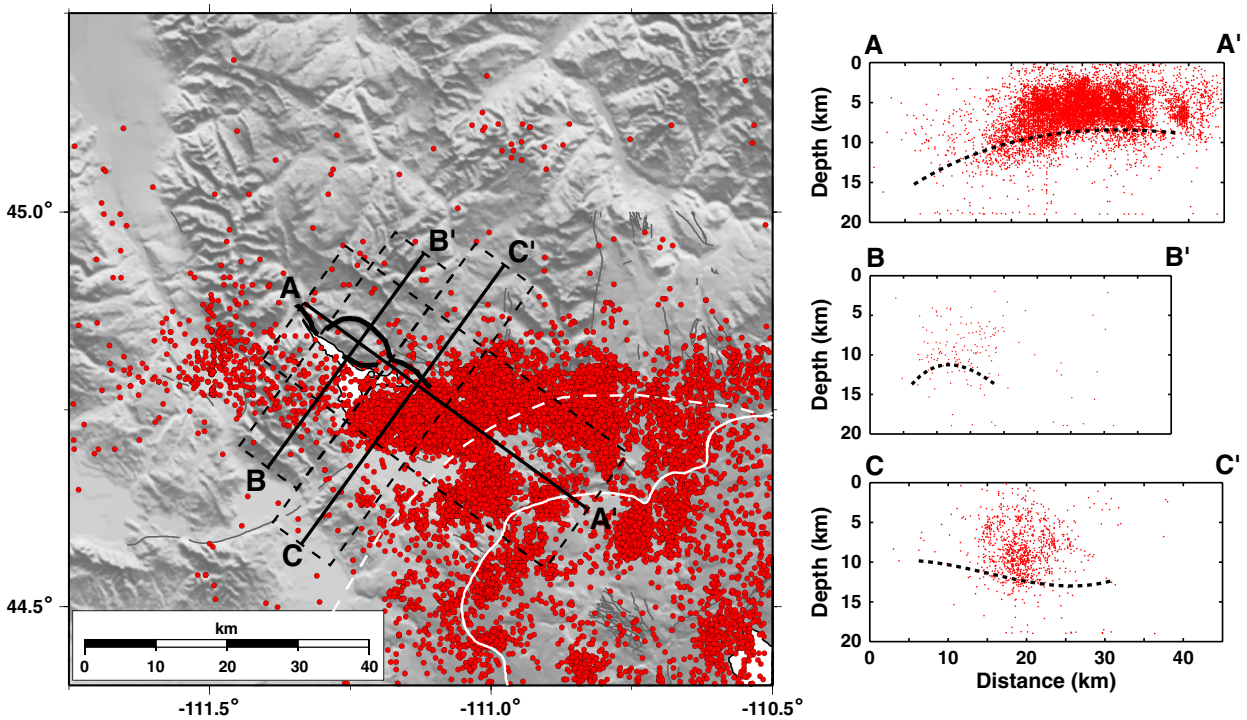

Figure 2. Locations of 1973–2011 earthquakes (gray dots) in the Yellowstone-Hebgen Lake area recorded by the University of Utah operated Yellowstone Seismic Network, with the 90th-percentile maximum focal-depths of three profiles shown by black dashed lines. Bold black lines represent the surface traces of the 1959 Hebgen Lake rupture.

orbit data from the Defense Mapping Agency and Scripps Institution of Oceanography were used. For each campaign, daily station positions and the covariance matrix were first solved for in the ITRF2005 reference frame and then combined to obtain average coordinates and baseline lengths by applying a technique of sequential least-squares estimation [*Brockmann*, 1996]. Readers are referred to *Puskas* [2000] and *Puskas et al*. [2007] for details on the GPS data processing of the Yellowstone-Hebgen Lake network.

[11] Recent studies suggest that white noise plus time-correlated color noise would be a more accurate noise model for GPS measurements [e.g., *Mao et al*., 1999, *Williams et al*., 2004]. For campaign style measurements separated in time by months to years, however, the short-term temporal correlations implied by color noise models should be less important than that for continuous data [*Williams et al*., 2004]. Our campaign GPS data were gathered in periods of no longer than 3 months in a single year, so that it would not be inappropriate to include only the white noise in the baseline measurements (see Table S1 in the Supporting Information).[1] For estimations of continuous GPS velocities, on the other hand, excluding the color noises would reflect approximately only the relative strength of the measurements but not realistic uncertainties.

3. Modeling of Postseismic Viscoelastic Relaxation for Lithospheric Rheology

3.1. Viscoelastic Deformation From Baseline Changes

[12] The measurements of eight baselines from the 1973–2000 trilateration and GPS surveys (Figure 3) were used to model the lithospheric rheology of the Hebgen Lake fault zone (data along with their 1-σ errors are summarized in the Supporting Information). Geodetic sites and baselines were chosen because: (1) They were occupied at least four times in the 1973–1987 trilateration or 1987–2000 GPS survey periods; (2) They are nearly orthogonal to the trace of the 1959 fault rupture so that relative postseismic motion between the hanging-wall and footwall of the fault can be best sampled; (3) The ground motion observations have relatively long time spans from 13 years up to 27 years. Note that three baselines, AIRP-HOLM, AIRP-BIGN, and BIGN-LION, have combined trilateration and GPS measurements

[1]All Supporting Information may be found in the online version of this article.

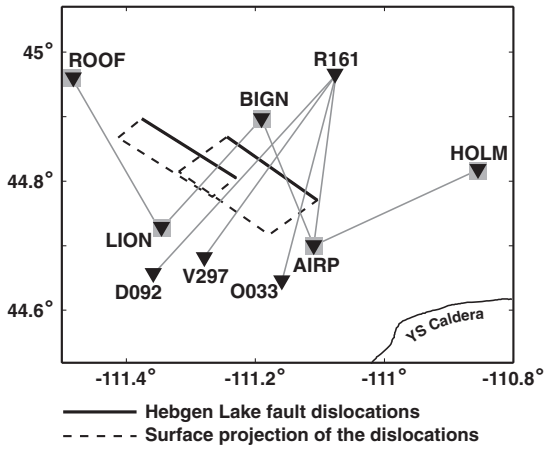

Figure 3. Geodetic stations and baselines used for rheologic modeling. Dashed rectangles show the surface projections of the 1959 Hebgen Lake fault dislocations [*Barrientos et al*., 1987].

overlapping in 1987 (Figure 3). *Savage et al*. [1996] determined that EDM-measured baselines were systematically longer, by a factor of 0.283 ± 0.100 parts per million, than the same baselines measured by GPS. We thus applied this correction to combine the two different geodetic observations into a consistent dataset (Table S1).

[13] Effects other than viscoelastic relaxation, such as afterslip and poroelastic rebound, may also contribute to the observed postseismic deformation. Afterslip can be the result of relaxation of a stress perturbation within the velocity-strengthening region when an earthquake propagates into that region from below [*Marone et al*., 1991], while poroelastic rebound can be produced by the postseismic relaxation of pore-fluid pressure gradients induced by the coseismic volume change of the country rock around the fault [e.g., *Peltzer et al*., 1998]. *Pollitz et al*. [2000], however, concluded that both afterslip and poroelastic rebound were minor contributions when considering the postseismic deformation pattern 3 years after the 1992 Lander earthquake. Because our geodetic observations were collected beginning 14 years after the 1959 Hebgen Lake main shock, these effects were not considered significant for our modeling analysis.

[14] Because geodetic measurements of surface deformation capture effects related to both time-invariant (tectonic) and transient (here the postseismic) processes, the former needs to be evaluated and removed when the latter is used to model the lithospheric rheology [e.g., *Hammond et al*., 2009]. We also assumed that the steady state tectonic deformation across the Hebgen Lake fault zone has been mainly the uniaxial southwest extension of the eastern Snake River Plain [*Puskas et al*., 2007], where an average extensional strain rate of ~0.027 μstrain/yr was estimated (see the Supporting Information).

3.2. Rheologic Modeling

[15] This study first implemented a two-layer model for the lithospheric rheology beneath the Hebgen Lake fault zone (Figure 4), with an elastic layer overlying a viscoelastic layer and a viscoelastic half-space. A linear Maxwell rheology was assumed for both the viscoelastic layer and half-space (see the Supporting Information). This working model of lithospheric rheology is consistent with a seismically accepted crustal model that the Conrad and Moho discontinuities are the rheologic and chemical boundaries separating the upper crust (elastic layer), lower crust (viscoelastic layer), and upper mantle (viscoelastic half-space), respectively.

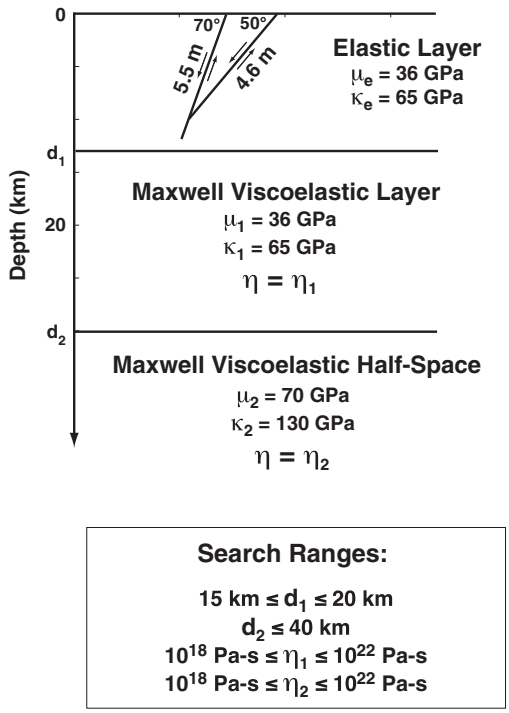

Figure 4. Fault and rheological model used for the Hebgen Lake earthquake and fault area. Four parameters, the depths, d_1 and d_2, and viscosities, η_1 and η_2, of two viscoelastic strata were evaluated by a Monte Carlo search. Fault source parameters are from *Doser* [1985]. The shear modulus, μ, and the bulk modulus, κ, were based on the average crust and upper mantle *P*-wave velocities of the Hebgen Lake-Yellowstone region [*Smith et al*., 1989]. The densities are 2800, 3100, and 3400 kg/m^3 for the elastic layer, viscoelastic layer, and half-space, respectively.

[16] Figure 4 shows a working dislocation model for the M_w 7.3 Hebgen Lake rupture based on the seismic moment tensor analysis of *Doser* [1985] and the geodetic models of *Barrientos et al*. [1987]. The elastic moduli were derived from the average crust and upper mantle *P*-wave velocities of the Hebgen Lake-Yellowstone region [*Smith et al*., 1989]. Two generally east to east-southeast striking fault segments ruptured during the main shock: (1) the southern Hebgen Lake segment is 18 km long, 15 km wide, with a dip of 70° SW and an average slip of 5.5 m, and (2) the northern Red Canyon segment is 18 km long, 12 km wide, with a dip of 50° SW and a slip of 4.6 m.

[17] The depths and viscosities of the two layers in Figure 4 were evaluated to best fit the temporal changes of baseline lengths across the Hebgen Lake fault (Figure 3). To do this we applied a Monte Carlo approach [e.g., *Spada*, 2001] in which a large set of a priori possible rheologic models were randomly selected for producing predictions of postseismic deformation field. Misfits between these forward results and the observations were then calculated and used to identify best fit models whose misfits are smaller than a given bound.

[18] A set of 20,000 rheologic models was generated spanning the range of plausible lithospheric conditions. For each model, four parameters were randomly selected in the ranges of 15–20 km and ≤40 km for the bottom depths of the two layers, d_1 and d_2, respectively, and 10^{18}–10^{22} Pa-s for both viscosities, η_1 and η_2 (Figure 4). The algorithm VISCO1D [*Pollitz*, 1997] was run for each model to estimate predicted rates of baseline change (see further discussions and examples of VISCO1D in the Supporting Information). For each baseline, a chi-squared, χ^2, function was employed to evaluate the misfit

$$\chi^2 = \frac{1}{N}\sum_{k=1}^{N}\left(\frac{\dot{L}_k^o - \dot{L}_k^m}{\sigma_k^o}\right)^2, \quad (1)$$

where $\dot{L}_k^o$ and $\dot{L}_k^m$ are the observed and predicted rates of baseline changes, σ_k^o is the one standard deviation uncertainty of the observation, and N is the number of surveys of the baseline. For each baseline in Figure 3, rheologic models with calculated χ^2 misfits within the lowest 5% interval were accepted. The models with acceptable fits to all eight baselines were considered to be the best fit models.

[19] Two best fit rheologic models, shown in Figure 5, were derived from the deformation measurements. For the baseline group Yellowstone (YS) that includes four baselines adjacent to the Yellowstone calderas (Figure 5a), the best fit models are characterized by a 9 km thick viscoelastic layer at 17 km depth with mean viscosities of 2×10^{19} Pa-s and 5×10^{18} Pa-s for the viscoelastic layer and half-space, respectively. The distributions of best fit models and the fitted curves of this group are shown in Figure 6. The mean viscosity of the lower crust is about four times higher than that of the upper mantle, and this difference is statistically significant based on a Student's *t*-test: the two-tailed probability p is 0.0012, indicating that there is a 98.8% chance of significantly different means. Here we define, by convention, the statistically significant difference of two means as being $p < 0.05$.

[20] Models for the baseline group Hebgen Lake fault (HLF) with baselines straddling the central and northwest Hebgen Lake fault zone (Figure 5b) reveal a thicker viscoelastic layer, ~15 km, and higher mean viscosities, 3×10^{21} and 2×10^{19} Pa-s for the lower crust layer and the upper mantle half-space, respectively, than those from the YS baseline group (Figure 7). These differences indicate a lateral variation of lithospheric rheology from northwest to the southeast in the Hebgen Lake-Yellowstone area, generally consistent with the large heat flow change from the Yellowstone caldera (>200 mW/m^2) to the Hebgen Lake fault zone (~130 mW/m^2, see later discussions).

[21] Note that the viscoelastic modeling algorithm used in this study [*Pollitz*, 1997] does not allow for fault dislocations to extend into the viscoelastic layer. Thus, the bottom depth of the elastic layer d_1, assumed as the upper bound of the brittle-ductile transition zone, has to be deeper than 15 km as constrained by the Hebgen Lake dislocation model (Figure 4). This constraint is consistent with the observed focal depth maxima distribution of the local seismicity (B-B′ in Figure 2). Possible spatial variations in the thickness of the brittle upper crust, which would be thinner than 15 km for areas with shallow seismicity and high surface heat flow, cannot be resolved. Nonetheless, we suggest that the lateral variation of rheologic properties beneath the Hebgen Lake fault zone implied by the GPS and trilateration observations are consistent with the local tectonic characteristics, in which shallow earthquake focal depths in addition to high temperatures and magmatic deformation sources of the

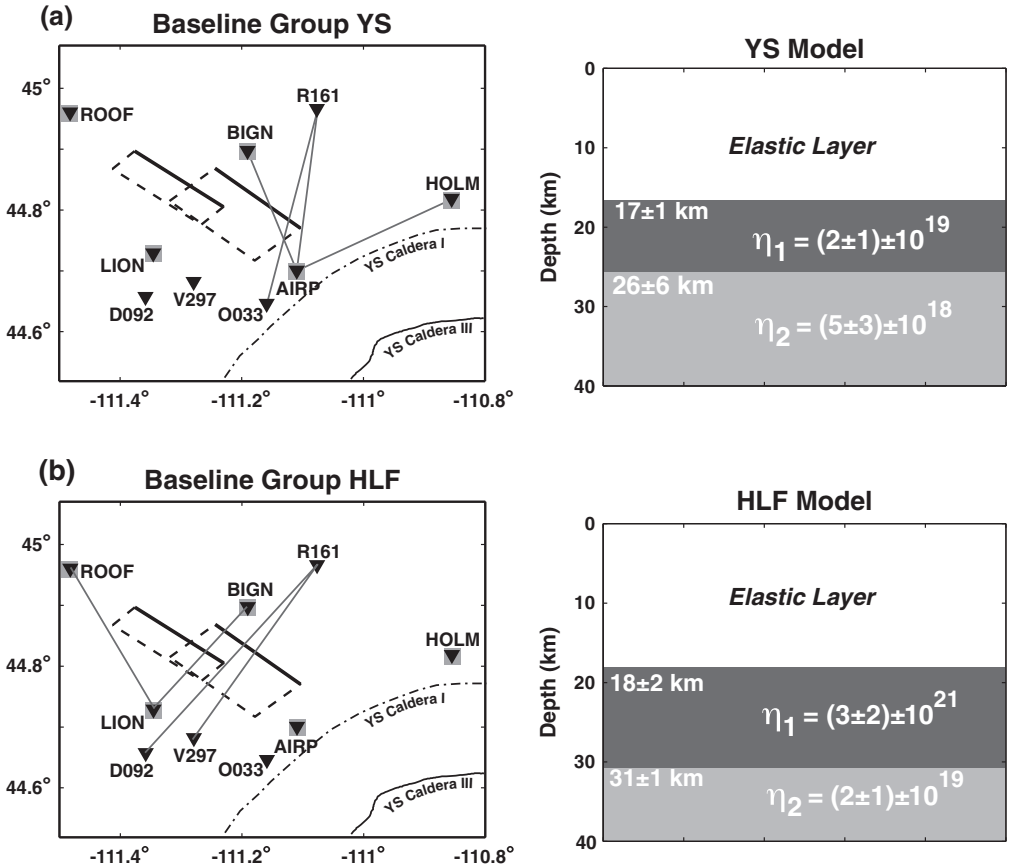

Figure 5. Best fit rheological models derived from horizontal baseline changes of GPS and EDM measurements. (a) For the area southeast of the Hebgen Lake fault zone near the Yellowstone caldera (YS model). (b) For the area across the central and northwestern Hebgen Lake fault (HLF model). Dark and light gray blocks represent the viscoelastic layer and half-space in Figure 4, respectively.

Yellowstone calderas correspond to a much hotter and thus weaker lower crust and upper mantle [*Smith and Braile*, 1994].

4. Discussion

4.1. Vertical Deformation From Precise Leveling Data

[22] While trilateration and GPS measure the horizontal and vertical deformation, leveling surveys provide additional constraints to measurements of vertical motion with higher precision, i.e., up to 0.1 mm/km. For a large normal-faulting earthquake similar to the 1959 Hebgen Lake event, the vertical component of postseismic deformation produced by the downward hanging-wall slip is the largest component of deformation. In this study we also included the vertical motion data of the Hebgen Lake region from three leveling routes [*Nishimura and Thatcher*, 2003], measured after the earthquake in 1959, 1960, 1964,1983, and 1987 near the epicentral area (G, H, and I; Figure 1).

[23] These leveling data were compared with vertical postseismic deformations predicted by different rheologic models. We selected these three leveling routes from among those in the Yellowstone-Hebgen Lake region because of their proximity to the rupture. These vertical-motion data are most likely related to transient tectonic deformation associated with the Hebgen Lake earthquake, rather than tectono-magmatic sources from the Yellowstone volcanic system.

[24] Figure 8 shows the leveling measurements plotted together with corresponding vertical displacements predicted by three rheologic models: (1) The YS model from baselines near the Yellowstone calderas (Figure 5a), (2) The HLF model from baselines across the central Hebgen Lake fault (Figure 5b), and (3) the single-layer model by *Nishimura and Thatcher* [2003]. The three models predict the observed vertical motion of leveling

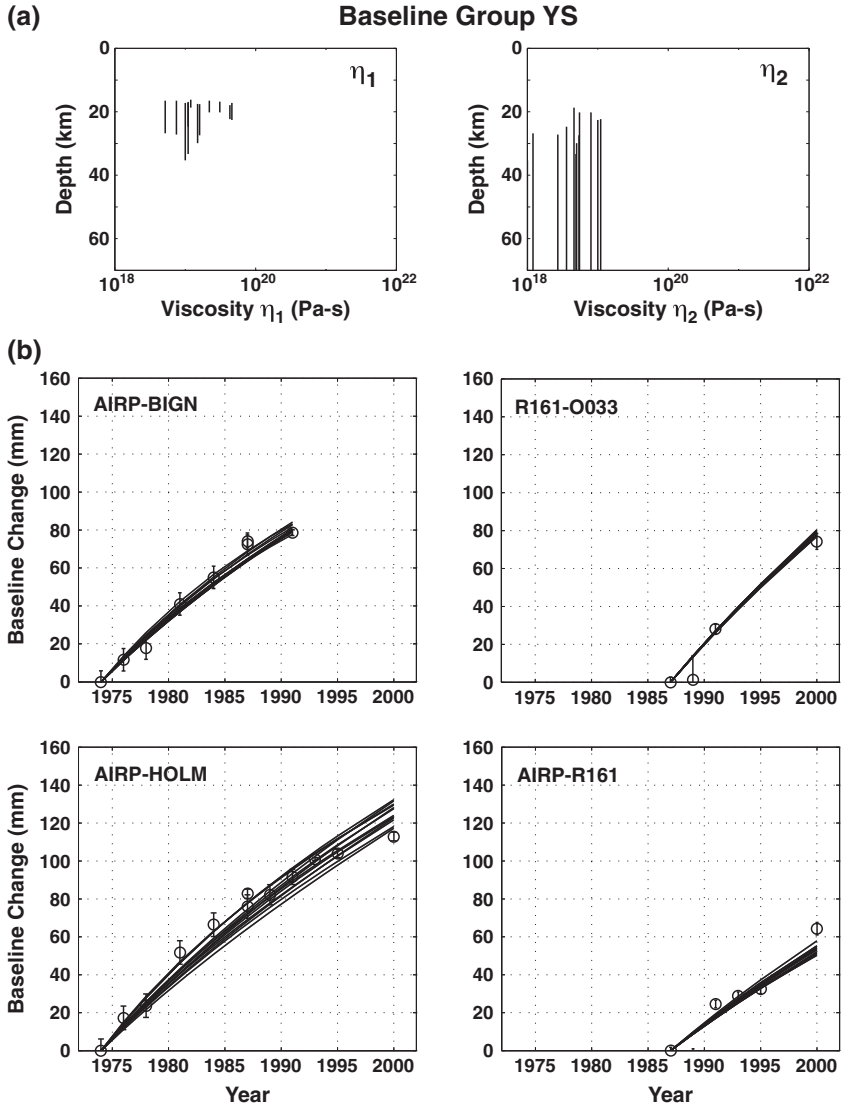

Figure 6. Best fit rheologic parameters of the Yellowstone model in Figure 5a. (a) Depth ranges of viscosity correspond to the thickness of the viscoelastic layer. Average values of viscosities and depths are shown in Figure 5. (b) Fit to baseline length changes. Circles with 1-σ error bars represent geodetic observations (EDM or GPS) and curves are derived from rheologic parameters shown in (a).

route G equally well, within 1σ error range. Models 2 and 3, however, predict the observations better than the YS model does for routes H and I along the footwall and hanging-wall of the fault, respectively. This result implies that the HLF model is more plausible for representing the lithospheric rheology across the Hebgen Lake fault than the YS mode, similar to the modeling results shown in the previous section.

[25] Nonetheless, the ~25 mm and >100 mm jumps at the north end of route G and the south end of route H, respectively (Figure 8), are not predicted by any of the three models. Note that both the G and H leveling data include measurements made one month after the 1959 Hebgen Lake main shock, thus afterslip occurring within this period would be included in the data and cannot be modeled by viscoelastic relaxation [*Nishimura and Thatcher*, 2003]. Edge effects caused by the approximation of rectangular dislocation models to the finite length fault planes [e.g., *Savage*, 1998] or other local disturbances such as ground water level change or benchmark instability may also contribute to these discrepancies.

4.2. Lithospheric Rheology and its Relation to the Youthful Yellowstone Volcanic System

[26] *Koseluk and Bischke* [1981] suggested that a crustal doming (vertical) rate of 3–5 mm/yr,

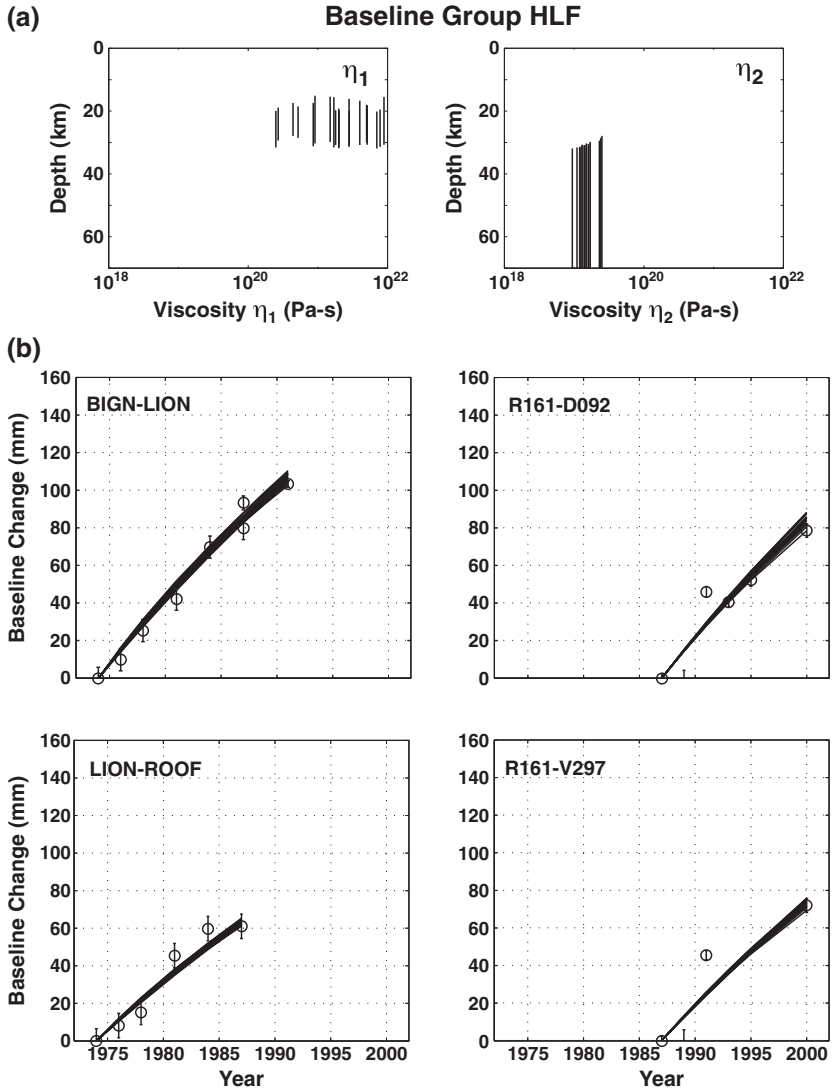

Figure 7. Best fit rheologic parameters of the Hebgen Lake fault model in Figure 5b. (a) Depth ranges of viscosity correspond to the thickness of the viscoelastic layer. (b) Fit to baseline length changes. See Figure 6 for more figure explanations.

measured by the initial leveling data from 1923 to 1960 around the Hebgen Lake fault and bracketing the earthquake aftershock zone [*Reilinger et al*., 1977], may have resulted from postseismic strain accumulation. Assuming a maximum stress drop of 400 bars for this earthquake, they obtained a viscosity of 2.3×10^{21} Pa-s below a 20 km thick elastic layer. Note that the stress-drop of the 1959 Hebgen Lake main shock determined by *Doser* [1985] from seismic data was smaller, ~150 bars, suggesting that *Koseluk and Bischke* [1981] results would overestimate the viscosity.

[27] *Reilinger* [1986] proposed models with a 30–40 km thick elastic layer overlying a viscoelastic half-space with a viscosity of $\sim 10^{19}$ Pa-s to fit the measurements of 1923, 1960, 1967, 1975, and 1983 vertical motion from a leveling route that passes within ~25 km of the epicenter of the Hebgen Lake earthquake (Figure 1). *Nishimura and Thatcher* [2003, 2004] derived similar results from the same leveling data as *Reilinger* [1986] plus data acquired in 1987 [*Holdahl and Dzurisin*, 1991], with an elastic thickness of 38 ± 8 km and a lower viscosity of $4 \times 10^{18 \pm 0.5}$ Pa-s for the half-space.

[28] Although the above studies suggested a single-layer rheologic model for the Hebgen Lake area, *Nishimura and Thatcher* [2003] modeled a viscoelastic lower crust with layer thickness of 18 km and viscosity greater than 1.2×10^{21} Pa-s that could satisfy the leveling data equally well. *Hammond et al*. [2009], in addition, proposed a preferred rheologic model with the viscosities of the lower crust

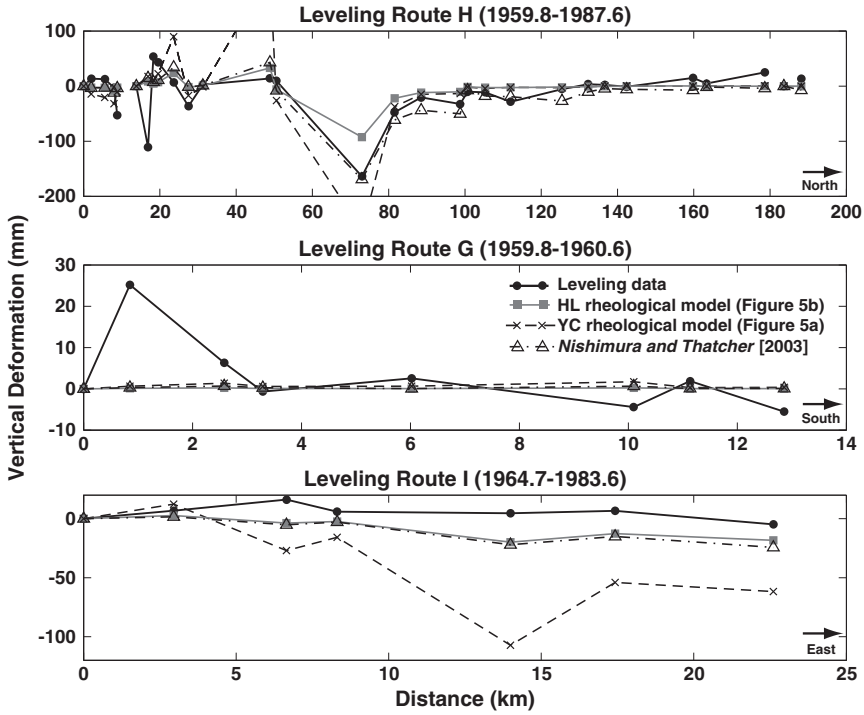

Figure 8. Vertical displacements observed along three leveling routes (see Figure 1) in the Hebgen Lake fault area. Observed data from 1959–1987 leveling surveys are shown by black dots, while predicted postseismic responses based on different rheological models are plotted by other symbols.

and upper mantle being $10^{20.5}$ and 10^{19} Pa-s, respectively, to best explain the postseismic relaxation measured by GPS and paleoseismic data in the Central Nevada seismic belt, an extensional stress regime that is similar to the Hebgen Lake area. These two results agree with our two-layer rheologic model for the fault zone (Figure 5) within the uncertainties of the model parameters and data. Moreover, results of the *t*-test showed significant differences between the lower crust and upper mantle viscosities of the HLF and YS rheologic models, which statistically support the assumption of two-layer structure for the Hebgen-Lake area.

[29] Although varying views of the distribution of Earth's rheological properties and strength have been proposed [e.g., *Bürgmann and Dresen*, 2008], our YS and HLF models imply a more viscous, or stronger, lower crust than the upper mantle. This result agrees with a hypothesis that the behavior of the continental lithosphere is dominated by the strength of its seismogenic layer, typically the upper crust, and that the continental mantle has no significant long-term strength [e.g., *Maggi et al.*, 2000]. *Thatcher and Pollitz* [2008], in addition, proposed that the upper mantle has an effective viscosity ~2 orders of magnitude less than the lower crust at time scales of postseismic and post-lake-filling relaxations (<~100 years). Our rheologic models were derived from surface deformation ~15–40 years following the earthquake and therefore are supported by the above conclusions.

[30] One explanation to the less viscous lower crust in the YS model than in the HBL model (Figure 5) can be the influence of crustal magma and related hydrothermal fluids associated with the northwestern Yellowstone caldera. *Jackson* [2002] has pointed out that the input of igneous melts and fluid into the lower crust can reduce the creep strength dramatically to cause transient lower crust flow. This proposition provides a plausible explanation for the lateral variation of our modeled rheologic structures, in which active hydrothermal features observed in the northwestern Yellowstone caldera may be responsible for a less viscous lower crust in the YS model.

[31] Temperature-dependent viscosity revealed by surface heat flow of the Yellowstone-Snake River Plain and the surrounding Basin and Range can also be responsible for the lateral variation of lithospheric rheology in the Hebgen Lake area. In the northwest of our study area, the borehole temperature measurements compiled by *Blackwell and*

Richards [2004] reveal a surface heat flow of ~90 mW/m^2, similar to that of the nearby Basin and Range. To the southeast of the Hebgen Lake fault zone, the heat flow data indicate higher values of ~130 mW/m^2 near the Yellowstone caldera boundary and >200 mW/m^2 in the caldera where direct measurements of 2000 mW/m^2, likely caused by the effects of hydrothermal convection, were recorded. Moreover, hypocenter locations of Yellowstone earthquakes show that the 90th percentile of the maximum focal depths range from 5 to 10 km in the surrounding area of Yellowstone-Snake River Plain and are less than 6 km beneath the caldera [*Farrell et al*., 2009; *Smith et al*., 2009]. The higher heat flow and shallower earthquake focal depths, implying hotter and weaker crustal rocks, in the southeast fault zone relative to the northwest are compatible with the lower viscosities inferred from the rheologic model close to the Yellowstone caldera (the YS model) than that across the fault (the HLF model).

[32] By combining the above data with rock type, strain rate, and gravity observations, *DeNosaquo et al*. [2009] provided lithospheric strength models for different thermal regimes of the Yellowstone area. Their models indicate that the depths of brittle-ductile transition in the upper crust and lower crust are about 11 and 27 km, respectively, in the area immediately adjacent to the Yellowstone caldera, within which the Hebgen Lake fault zone is approximately located. Although the comparison between brittle-ductile transition from earthquake focal depths [*DeNosaquo et al*., 2009] and rock rheology from postseismic stress relaxation (this study) may not be direct, both results consistently show a ductile lithosphere beneath the Hebgen Lake fault zone at depths greater than ~20 km.

4.3. Contemporary Postseismic Relaxation in the Yellowstone-Snake River Plain Region

[33] The 1959 Hebgen Lake, MT, and the 1983 Borah Peak, ID, earthquakes were the largest historic earthquakes in the Yellowstone-Snake River Plain region and thus expected to produce measurable postseismic deformation in the area. In this section we applied our derived rheologic model (HLF model, Figure 5b) to evaluate the horizontal postseismic velocities produced by these two large events and then compared results with contemporary deformation measured by GPS from 2005 to 2011. For the Borah Peak earthquake, a dislocation model from *Barrientos et al*. [1987] based on mapped fault scarps and leveling data was used: an 18 km long and 18 km wide fault area and 2.1 m of coseismic slip for the southern segment, and 8 km, 8 km, 1.4 m for the northern segment. These two segments are the main parts of the Lost River fault on which the earthquake occurred.

[34] Figure 9 shows the combined postseismic velocities of the two events and the measured contemporary horizontal deformation at continuous GPS sites in the Yellowstone-Snake River Plain region from 2005 to 2011. Note that the postseismic velocities are relative to the fixed fault planes of each earthquake, while the GPS velocities are referenced in a stable North American framework. Therefore, we compared the two motions based on relative velocities of GPS stations across the faults (Figure 10).

[35] Figures 9 and 10a reveal that in the Hebgen Lake area the postseismic motions of P461-P458 and P460-P458 are notable components, ~70%, of the observed ground deformation, suggesting that the viscoelastic relaxation is a major transient effect of the regional (>50 km) extension across the fault. In a short range of ~30 km across the fault between stations P456, P457, and P712 and station P458, however, postseismic relaxation appears to be a smaller effect, but still ~30%, to the current deformation where high NNE-SSW extensional rates of ~3 mm/yr were revealed by GPS velocities (Figure 10a). This extension may be partly caused by the ongoing earthquake activity between the Hebgen Lake fault and the Yellowstone caldera (Figure 2); for example the 1985 earthquake swarm across the northwest caldera boundary [*Waite and Smith*, 2002]. South of station P676 into the Snake River Plain, the postseismic motion decreases to less than 10% of the contemporary extensional rate of ~2–3 mm/yr (Figure 9). We therefore suggest that the postseismic relaxation produced a significant transient signal in the local horizontal velocity and strain field of the northwest Yellowstone and northeast Snake River Plain.

[36] In the 1983 Borah Peak epicentral area, the postseismic relaxation produces nearly the same motion as the regional extension measured by GPS, ~1 mm/yr in the NE-SW direction between the footwall (stations P357 and P355) and hanging wall (stations P352, P353, and 354) of the fault (Figure 10b). Recall that the HLF rheologic model was applied to estimate the postseismic motion; therefore, the changes of the lithospheric structures between the Hebgen Lake and Borah Peak areas

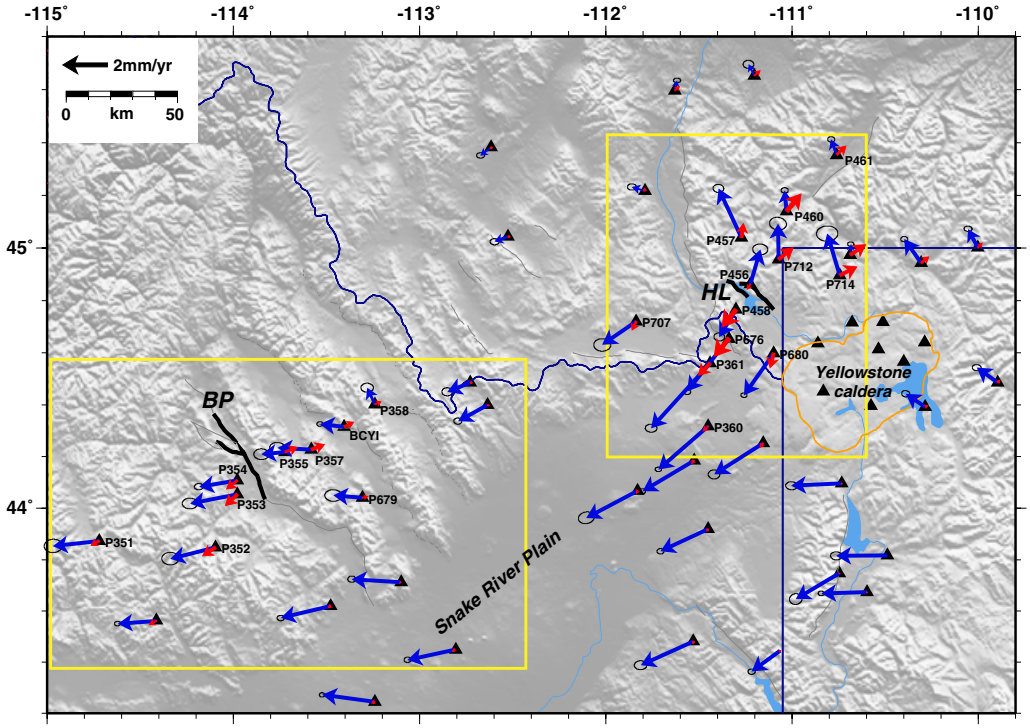

Figure 9. Postseismic horizontal deformation (red arrows) in the Yellowstone-Snake River Plain region caused by viscoelastic relaxations of the 1959 M_w 7.3 Hebgen Lake, MT, (HL) and the 1983 M_w 6.9 Borah Peak, ID, (BP) earthquakes. Blue arrows show horizontal velocities (with 2-σ error ellipses) measured by continuous GPS stations (black triangles). All motions were calculated or observed from 2005 to 2011. Note that the postseismic velocities are relative to the fault planes of the two earthquakes, while the GPS velocities are in a stable North American reference frame. Yellow boxes outline the areas shown in Figure 10.

were not taken into account. In addition, most GPS stations of the Borah Peak network only began to operate in mid-2008, so a longer data window may be needed to resolve the relatively slow, and possibly time-dependent, tectonic motion in the area more confidently. Despite these factors, our results suggest that the contemporary ground motion across the 1983 Borah Peak epicentral area in the central Snake River Plain is primarily the effect of viscoelastic postseismic relaxation.

4.4. Postseismic Response Applied to the Wasatch Fault Zone, Utah

[37] In this section, we evaluate the postseismic responses induced by large paleo- and historic earthquakes of the Wasatch fault zone in Utah that is in a similar seismogenic extensional regime as the Hebgen Lake and Borah Peak earthquakes. Rheologic working models derived from different geological observations in the area are first discussed.

[38] Based on the ages and elevations of the uplifted shorelines of Quaternary Lake Bonneville rebound in Utah, several studies have proposed similar single-layer rheologic models with an elastic crustal thickness of 25–30 km and mantle viscosity of 1–3 $\times 10^{19}$ Pa-s [*Nakiboglu and Lambeck*, 1983; *Bills and May*, 1987; *Bills et al.*, 1994]. *Bills et al.* [1994], in addition, indicated that there was no compelling evidence for a rheology more complex than the classic Maxwell model.

[39] We first employed a single-layer rheologic structure, $d = 25$ km and $\eta = 2 \times 10^{19}$ Pa-s, to the Wasatch fault and adjacent East Great Salt Lake fault where six Holocene paleoearthquakes occurred 500–1200 years ago [*McCalpin and Nishenko*, 1996; *Dinter and Pechmann*, 2001; *DuRoss et al.* 2011], and three historic earthquakes were considered as possible contributors of postseismic signal to the current deformation field (Figure 11). The six paleoearthquakes include the most recent ruptures on five of the Wasatch fault segments and the East Great Salt Lake fault. The three historic earthquakes are the M_w 6.6 1934 Hansel Valley, UT, the M_w 5.6 1962 Cache Valley, UT, and the M_w 6.2 1975 Pocatello Valley, ID, earthquakes. We

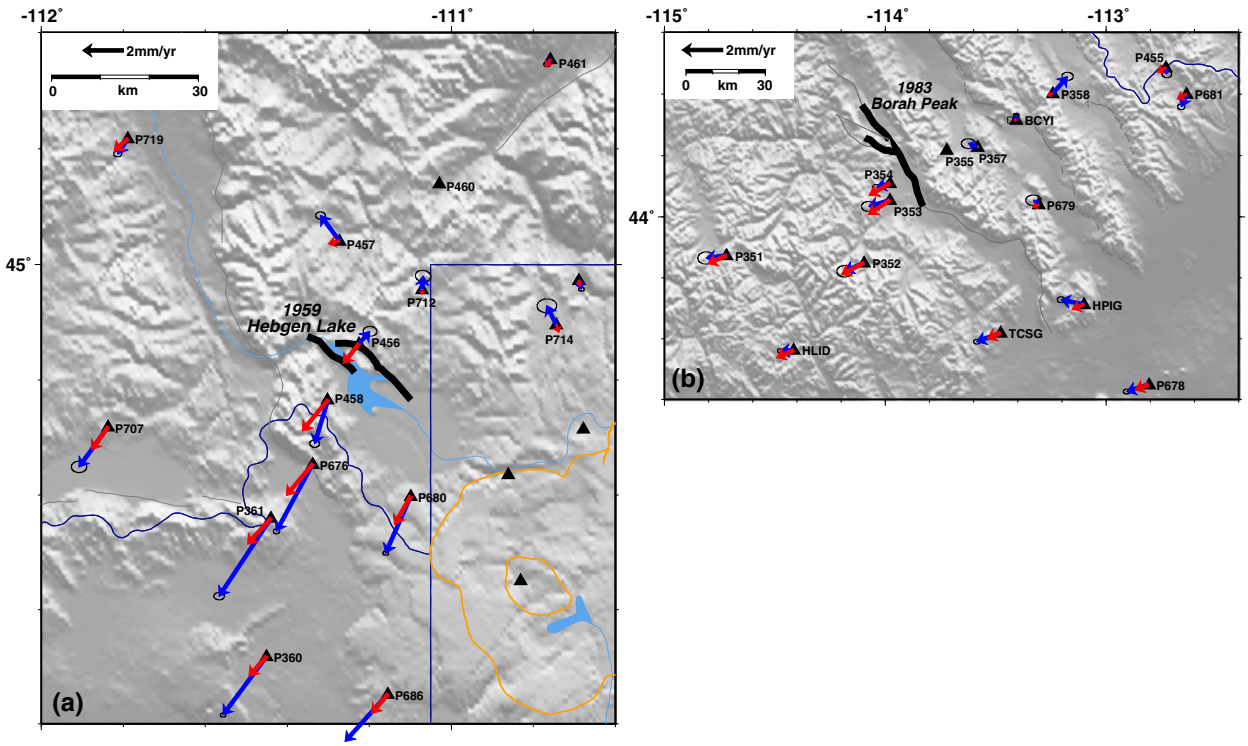

Figure 10. Modeled postseismic deformation (red arrows) and GPS-observed ground motion (blue arrows): (a) Relative to station P460 in the 1959 Hebgen Lake epicentral area; (b) Relative to station P355 in the 1983 Borah Peak epicentral area. See more map descriptions in Figure 9.

employed paleoearthquake single-segment rupture models for the Wasatch fault based on *Chang and Smith* [2002], with the historic earthquakes and parameters listed in Table 1.

[40] Figure 11 shows the horizontal postseismic motion (green arrows) of the Wasatch Front area produced by these earthquakes. Results show that the *M* 6.6 Hansel Valley, UT, earthquake and the largest paleo-rupture on the Wasatch fault, ~500 years B.P. on a central segment of the Wasatch fault [*McCalpin and Nishenko*, 1996], are the dominant sources of the contemporary postseismic deformation. The point velocities, however, do not exceed 0.1 mm/yr, with relative velocities less than 0.2 mm/yr across the fault. These motions are smaller than the GPS-measured extensional rates of the Wasatch Front of ~1–3 mm/yr [*Martinez, et al.*, 1998; *Thatcher et al.*, 1999; *Bennett et al.*, 2003; *Hammond and Thatcher*, 2004; *Chang et al.*, 2006] and are within the uncertainties of horizontal velocities of 0.1–0.2 mm/yr determined by continuous GPS in the Basin and Range [*Davis et al.*, 2003].

[41] For an independent evaluation we implemented the two-layer HLF model described earlier (Figure 5b) as another rheologic working model. In addition to the similar extensional-stress regime and normal-faulting earthquake mechanisms observed in these two areas, comparable lithospheric rheology revealed by different independent observations also support the use of the HLF model to the Wasatch Front area. For example, lithospheric structures based on the Lake Bonneville deformed shoreline were characterized by a viscoelastic lower crust layer at 10–40 km depth with viscosity in a range of 10^{20}–10^{21} Pa-s [*Bills et al.*, 1994]. The viscosity of the mantle half-space from this study is ~10^{19} Pa-s, similar to that obtained by *Nakiboglu and Lambeck* [1983] and *Bills and May* [1987] from isostatic rebound of Lake Bonneville. *Gourmelen and Amelung* [2005] and *Hammond et al.* [2009] also derived similar rheologic models to best explain postseismic deformations in the Central Nevada seismic belt of the western Basin and Range.

[42] In addition, the depth to the viscoelastic half-space of the HLF model, ~30 km (Figure 5b), is consistent with a Moho depth for the eastern Basin and Range [*Smith and Bruhn*, 1984]. The low half-space viscosity, ~10^{19} Pa-s, may indicate a weaker upper mantle, which is implied by the averaged high surface

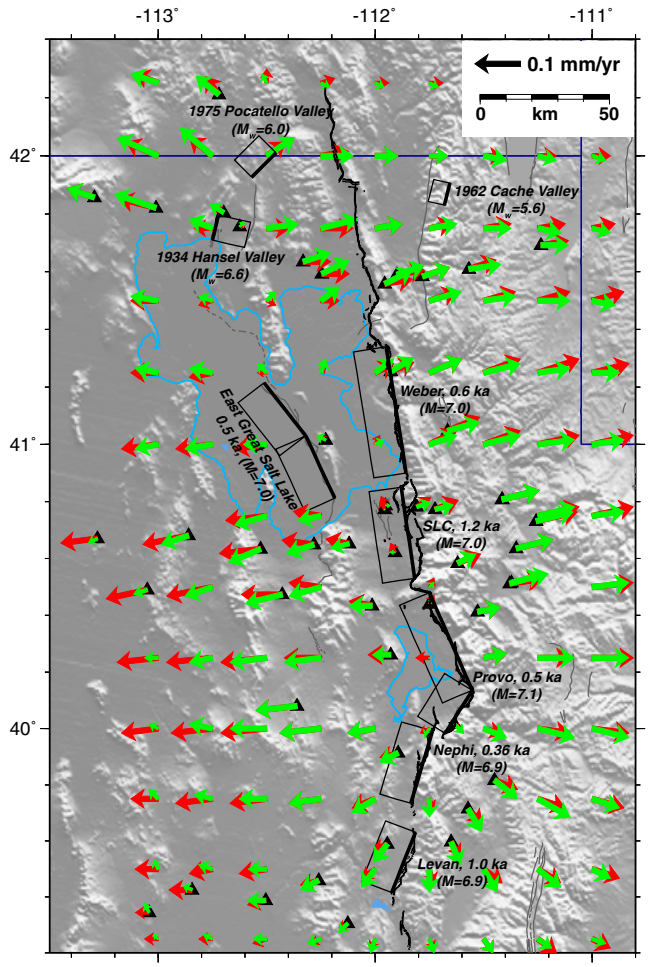

Figure 11. Contemporary postseismic horizontal velocities of the Wasatch Front, Utah, induced by large prehistoric and historic earthquakes. Fault dislocation models for the six youngest late-Quaternary paleoearthquakes and three historic events of the area are shown by rectangles, with thick lines indicating upper dip directions. Green and red arrows show results based on rheological working models from the Lake Bonneville rebound and the Hebgen Lake postseismic relaxation (HLF model, Figure 5b), respectively. Black lines highlight the Wasatch fault, and gray lines represent Quaternary faults. Triangles show locations of continuous GPS stations. Note that the velocity scale is 0.1 mm/yr.

heat-flow, 90–100 mW/m^2, observed in the Basin and Range of Utah [*Powell*, 1997; *Henrikson*, 2000].

[43] Figure 11 shows the horizontal postseismic velocities inferred from the two-layer HLF model. Similar to the results from the above Lake Bonneville rheologic model, the magnitudes of these motions are smaller than 0.1 mm/yr and are therefore less than 10% of the GPS-measured deformation rates in the Wasatch Front area. Alternatively, *Malservisi et al.* [2003] used finite element models with laterally

Table 1. Dislocation Models for Large Historic Earthquakes of the Wasatch Front

Earthquake	Length (km)	Top Depth (km)	Bottom Depth (km)	Dip (deg)	Rake (deg)	Slip (cm)
1934 M_w 6.6 Hansel Valley, UT[a,b]	10	0	11	50°E	90°	57
1962 M_w 5.6 Cache Valley, UT[c]	8	4	10	43°W	102°	12
1975 M_w 6.0 Pocatello Valley, ID[d,e]	13	2	9	39°W	53°	50

[a]*Chen* [1988].
[b]*Doser* [1989].
[c]*Westaway and Smith* [1989].
[d]*Bache et al.* [1980].
[e]*Arabasz et al.* [1981].

varied lithospheric rheology across the Wasatch fault to evaluate earthquake cycle effects of large Wasatch paleoearthquakes. Their results indicate that the viscoelastic effects near the fault are completely relaxed at present due to the long earthquake recurrence time and the long time elapsed since the last earthquake, consistent with that shown in Figure 11. We therefore propose that postseismic relaxation has relatively small effects on the contemporary horizontal deformation field across the Wasatch fault zone. Other tectonic processes such as the interseismic loading of faults are likely the main sources responsible for the current deformation of the region.

5. Conclusions

[44] Time-dependent changes in surface deformation following the 1959 M_w 7.3 Hebgen Lake, MT, earthquake, assessed by trilateration and GPS from 1973 to 2000, were used to estimate lithospheric rheology associated with this normal-faulting area. These data were augmented by vertical deformation data from leveling for the period of 1923 to 1987. Working models for the lithosphere included an elastic layer overlying a viscoelastic layer and half-space. Two best fit models were found: (1) the Hebgen Lake fault (HLF) model from baselines across the central fault zone, and (2) the Yellowstone (YS) model from baselines at the southeast end of the fault near the Yellowstone calderas, with the latter represents a weaker, less viscous, lower crust and upper mantle than the former. This lateral variation can be explained by the proximity of the southeastern end of the Hebgen Lake fault to the Yellowstone volcanic field, where very high heat flow and a thin seismogenic layer have been observed. Employing laterally heterogeneous viscoelastic models [e.g., *Pollitz*, 2003b] is thus necessary for future studies to approach the three-dimensional structure of lithospheric rheology of the Hebgen Lake-Yellowstone area.

[45] Combined postseismic deformation of the Yellowstone-Snake River Plain produced by the Hebgen Lake and the 1983 M_w 6.9 Borah Peak, ID, earthquakes was estimated based on the above HLF model. Comparison of the results with the contemporary velocity field from continuous GPS data suggests that the postseismic relaxation is a notable signal in the horizontal deformation field of the northwest Yellowstone and the eastern Snake River Plain.

[46] Rheologic models from the Hebgen Lake region and the Late Quaternary rebound of Lake Bonneville in the eastern Basin and Range were both examined to evaluate the combined postseismic relaxation of six paleoearthquakes and three $M \geq 5.6$ historic events in the Wasatch Front area. With horizontal motion smaller than 0.1 mm/yr, the postseismic deformation thus has minor effects on the contemporary E-W horizontal deformation of the Wasatch fault zone observed by GPS of ~1–3 mm/yr.

Acknowledgments

[47] We thank Fred Pollitz for providing the computer code VISCO1D. Jim Savage provided the trilateration data, and Chuck Meertens provided insights into GPS data acquisition and processing. Leveling data from Takuya Nishimura and Wayne Thatcher benefited this paper. Special thanks to Bill Hammond for revising the manuscript, and Robert Reilinger and Rick Bennett for reviewing the paper and providing valuable comments. This research was funded by the U.S. Geological Survey (NEHRP 02HQGR-0098), the NSF Continental Dynamics Program (EAR-0314237), the National Science Council of Taiwan (99-2116-M-008-033), and The Brinson Foundation. Computation support was in part provided by the Center for High Performance Computing of the University of Utah.

References

Arabasz, W. J., W. D. Richins, and C. J. Langer (1981), The Pocatello Valley (Idaho-Utah border) earthquake sequence of March to April 1975, *Bull. Seismol. Soc. Am. 71*, 803–826.

Bache, T. C., D. G. Lambert, and T. G. Barker (1980), A source model for the March 28, 1975, Pocatello Valley earthquake from time-domain modeling of teleseismic P waves, *Bull. Seismol. Soc. Am. 70*, 405–818.

Barrientos, S. E., R. S. Stein, and S. N. Ward (1987), Comparison of the 1959 Hebgen Lake, Montana and the 1983 Borah Peak, Idaho, earthquakes from geodetic observations, *Bull. Seismol. Soc. Am. 77*, 784–808.

Bennett, R. A., B. P. Wernicke, N. A. Niemi, A. M. Friedrich, and J. L. Davis (2003), Contemporary strain rates in the northern Basin and Range province from GPS data, *Tectonics*, *22*, doi:10.1029/2001TC001355.

Bills, B. G., and G. M. May (1987), Lake Bonneville: Constrains on lithospheric thickness and upper mantle viscosity from isostatic warping of Bonneville, Provo, and Gilbert stage shorelines, *J. Geophys. Res.*, *92*, 11,493–11,508.

Bills, B. G., D. R. Currey, and G. A. Marshall (1994), Viscosity estimates for the crust and upper mantle from patterns of lacustrine shoreline deformation in the Eastern Great Basin, *J. Geophys. Res.*, *99*, 22,059–22,086.

Blackwell, D. D., and M. C. Richards (2004), Geothermal map of North America. *Am. Assoc. Petroleum Geologist*, scale:1:6,500,000.

Brockmann, E. (1996), Combination of solutions for geodetic and geodynamic applications of the Global Positioning System (GPS), Ph.D. dissertation, Astronomical Institute, University of Berne, Berne, Switzerland, 211 pp.

Bürgmann, R., and G. Dresen (2008), Rheology of the lower crust and upper mantle: Evidence from rock mechanics, geodesy, and field observations, *Annu. Rev. Earth Planet. Sci.*, *36*, doi:10.1146/annurev.earth.36.031207.124326, 531–567.

Chang, W.-L., and R. B. Smith (2002), Integrated seismic-hazard analysis of the Wasatch Front, Utah, *Bull. Seismol. Soc. Am.*, *92*, 1904–1922, doi:10.1785/0120010181.

Chang, W.-L., R. B. Smith, C. M. Meertens, and R. B. Harris (2006), Contemporary deformation of the Wasatch fault, Utah, from GPS measurements with implications for interseismic fault behavior and earthquake hazard: Observations and kinematic analysis, *J. Geophys. Res.*, *111*, 19, doi:10.1029/2006JB004326.

Chang, W.-L., R. B. Smith, J. Farrell, and C. M. Puskas (2010), An extraordinary episode of Yellowstone caldera uplift, 2004–2010, from GPS and InSAR observations, *Geophys. Res. Lett.*, *37*, L23302, doi:10.1029/2010GL045451.

Chen, G. J. (1988), A study of seismicity and spectral source characteristics of small earthquakes: Hansel Valley, Utah, and Pocatello Valley, Idaho, areas, M.S. Thesis, University of Utah, Salt Lake City, Utah, 119 pp.

Davis, J. L., R. A. Bennett, and B. P. Wernicke (2003), Assessment of GPS velocity accuracy for the Basin and Range Geodetic Network (BARGEN), *Geophys. Res. Lett.*, *30*, 1411, doi:10.1029/2003GL016961.

DeNosaquo, K. R., R. B. Smith, and A. R. Lowry (2009), Density and lithospheric strength models of the Yellowstone-Snake River Plain volcanic system from gravity and heat flow data, *J. Volcanol. Geotherm. Res.*, *188*, 108–127.

Dinter, D. A., and J. C. Pechmann (2001), Seismic risk in the Wasatch Front region, Utah, from the East Great Salt Lake normal fault: Estimates from high resolution seismic reflection data, *Geol. Soc. Am. Abs. with Progs.*, *33*(6), A346.

Doser, D. I. (1985), Source parameters and faulting processes of the 1959 Hebgen Lake, Montana, earthquake sequence, *J. Geophys. Res.*, *90*, 4537–4555.

Doser, D. I. (1989). Extensional tectonics in northern Utah-southern Idaho, U.S.A., and the 1934 Hansel Valley sequence, *Phys. Earth Planet. Inter.*, *48*, 64–72.

DuRoss, C. B., S. F. Personius, A. J. Crone, S. S. Olig, and W. R. Lund (2011), Integration of paleoseismic data from multiple sites to develop an objective earthquake chronology: Application to the Weber segment of the Wasatch fault zone, Utah, *Bull. Seismol. Soc. Am.*, *101*, 2765–2781, doi: 10.1785/0120110102.

Farrell, J., R. B. Smith, T. Taira, W.-L. Chang, and C. M. Puskas (2009), Dynamics and rapid migration of the energetic 2008–2009 Yellowstone Lake earthquake swarm, *Geophys. Res. Lett.*, *37*, L19305, doi:10.1029/2010GL044605.

Freed, A. M., and R. Bürgmann (2004), Evidence of power-law flow in the Mojave Desert mantle, *Nature*, *430*, 548–551.

Gourmelen N., and F. Amelung (2005), Postseismic mantle relaxation in the Central Nevada Seismic Belt, *Science*, *310*, 1473, doi:10.1126/science.1119798.

Hammond, W. C., and W. Thatcher (2004), Contemporary deformation of the Basin and Range province, western United States: 10 years of observation with the Global Positioning System, *J. Geophys. Res.*, *109*, doi:10.1029/2003JB002746.

Hammond, W. C., C. Kreemer, and G. Blewitt (2009), Geodetic constraints on contemporary deformation in the northern Walker Lane: 3. Postseismic relaxation in the Central Nevada Seismic Belt, in *Late Cenozoic Structure and Evolution of the Great Basin–Sierra Nevada Transition*, edited by J. S. Oldow and P. Cashman, *Spec. Pap. Geol. Soc. Am.*, *447*, 33–54, doi:10.1130/2009.2447(03).

Henrikson, A. (2000), New heat flow determinations from oil and gas wells in the Colorado Plateau and Basin and Range of Utah, M.S. Thesis, University of Utah, Salt Lake City, Utah, 70 pp.

Holdahl, S. R., and D. Dzurisin (1991), Time-dependent models of vertical deformation for the Yellowstone-Hebgen Lake region, 1923-1987, *J. Geophys. Res.*, *96*, 2465–2483.

Hugentobler, U., S. Schaer, and P. Fridez (2001), Bernese GPS software version 4.2, Astronomical Institute, University of Berne, 511 pp.

Husen, S., and R. B. Smith (2004), Probabilistic earthquake relocation in three-dimensional velocity models for the Yellowstone National Park region, Wyoming, *Bull. Seismol. Soc. Am.*, *94*, 880–896.

Jackson, J. (2002), Strength of the continental lithosphere: Time to abandon the jelly sandwich, *GSA Today*, *12*, 4–10.

Koseluk, R. A., and R. E. Bischke (1981), An elastic rebound model for normal fault earthquakes, *J. Geophys. Res.*, *86*, 1081–1090.

Maggi, A., J. A. Jackson, D. McKenzie, and K. Priestley (2000), Earthquake focal depth, effective elastic thickness, and the strength of the continental lithosphere, *Geology*, *28*, 495–498.

Malservisi, R., T. H. Dixon, P. C. La Femina, and K. P. Furlong (2003), Holocene slip rate of the Wasatch fault zone, Utah, from geodetic data: Earthquake cycle effects, *Geophys. Res. Lett.*, *30*(13), 1673, doi:10.1029/2003GL017408.

Mao, A., C. G. A. Harrison, and T. H. Dixon (1999), Noise in GPS coordinate time series, *J. Geophys. Res.*, *104*, 2797–2816.

Marone, C. J., C. H. Scholtz, and R. Bilham (1991), On the mechanics of earthquake afterslip, *J. Geophys. Res.*, *96*, 8441–8452.

Martinez, L., C. M. Meertens, and R. B. Smith (1998), Rapid deformation rates along the Wasatch fault zone, Utah, from first GPS measurements with implications for earthquake hazard, *Geophys. Res. Lett.*, *25*, 567–570.

McCalpin, J. P., and S. P. Nishenko (1996), Holocene paleoseismicity, temporal clustering, and probabilities of future large ($M > 7$) earthquakes on the Wasatch fault zone, Utah, *J. Geophys. Res.*, *101*, 6233–6253.

Nakiboglu, S. M., and K. Lambeck (1983), A reevaluation of the isostatic rebound of Lake Bonneville, *J. Geophys. Res.*, *88*, 10,439–10,447.

Nishimura, T., and W. Thatcher (2003), Rheology of the lithosphere inferred from postseismic uplift following the 1959 Hebgen Lake earthquake, *J. Geophys. Res.*, *108*, doi:10.1029/2002JB002191.

Nishimura, T., and W. Thatcher (2004), Correction to "Rheology of the lithosphere inferred from postseismic uplift following the 1959 Hebgen Lake earthquake", *J. Geophys. Res.*, *109*, doi:10.1029/2003JB002798.

Peltzer, G., P. Rosen, F. Rogez, and K. Hudnut (1998), Poroelastic rebound along the Landers 1992 earthquake surface rupture, *J. Geophys. Res.*, *103*, 30,131–30,145.

Pollitz, F. F. (1997), Gravitational-viscoelastic postseismic relaxation on a layered spherical Earth, *J. Geophys. Res.*, *102*, 17,921–17,941.

Pollitz, F. F. (2003a), Transient rheology of the uppermost mantle beneath the Mojave Desert, California, *Earth Planet. Sci. Lett.*, *215*, 89–104.

Pollitz, F. F. (2003b), Post-seismic relaxation theory on a laterally heterogeneous viscoelastic model, *Geophys. J. Int.*, *155*, 57–78.

Pollitz, F. F., G. Peltzer, and R. Burgmann (2000), Mobility of continental mantle: Evidence from postseismic geodetic observation following the 1992 Landers earthquake, *J. Geophys. Res.*, *105*, 8035–8054.

Powell, W. G. (1997), Thermal state of the lithosphere in the Colorado Plateau-Basin and Range transition zone, Utah,

Ph.D. Dissertation, University of Utah, Salt Lake City, Utah, 232 pp.

Puskas, C. M. (2000), Deformation of the Yellowstone caldera, Hebgen Lake fault zone, and eastern Snake River Plain from the Global Positioning System, seismicity, and moment release, M.S. Thesis, University of Utah, Salt Lake City, Utah, 150 pp.

Puskas, C., R. B. Smith, C. M. Meertens, and W. L. Chang (2007), Crustal deformation of the Yellowstone-Snake River Plain volcano-tectonic system: Campaign and continuous GPS observations, 1987–2004, *J. Geophys. Res.*, *112*, B03401, doi:10.1029/2006JB004325.

Reilinger R. (1986), Evidence for postseismic viscoelastic relaxation following the 1959 M = 7.5 Hebgen Lake, Montana, earthquake, *J. Geophys. Res.*, *91*, 9488–9494.

Reilinger R. E., G. P. Citron, and L. D. Brown (1977), Recent vertical crustal movements from precise leveling data in southwestern Montana, western Yellowstone National Park, and the Snake River plain, *J. Geophys. Res.*, *82*, 5349–5359.

Savage, J. C. (1998), Displacement field for an edge dislocation in a layered half-space, *J. Geophys. Res.*, *103*, 2439–2446.

Savage, J. C., M. Lisowski, W. H. Prescott, and A. M. Pitt (1993), Deformation from 1973 to 1987 in the epicentral area of the 1959 Hebgen Lake, Montana, earthquake (M_s = 7.5), *J. Geophys. Res.*, *98*, 2145–2153.

Savage, J. C., M. Lisowski, and W. H. Prescott (1996), Observed discrepancy between Geodolite and GPS distance measurements, *J. Geophys. Res.*, *101*, 25547–25552.

Smith, R. B., and M. L. Sbar (1974), Contemporary tectonics and seismicity of the western United States with emphasis on the Intermountain Seismic Belt, *Geol. Soc. Am. Bull.*, *85*, 1205–1218.

Smith, R. B., and R. L. Bruhn (1984), Intraplate extensional tectonics of the eastern Basin-Range: Inferences on structural style from seismic reflection data, regional tectonics, and thermal-mechanical models of brittle-ductile deformation, *J. Geophys. Res.*, *89*, 5733–5762.

Smith, R. B., W. C. Nagy, K. A. Julander, J. J. Viveiros, C. A. Barker, and D. G. Gants (1989), Geophysical and tectonic framework of the eastern Basin and Range-Colorado Plateau-Rocky Mountain transition, in *Geophysical Framework of the Continental United States*, edited by L. C. Pakiser and W. D. Mooney, *Geol. Soc. Am. Memoir*, *172*, 205–233.

Smith, R. B., and L. W. Braile (1994), The Yellowstone hotspot, *J. Volcanol. Geotherm. Res. 61*, 121–187.

Smith, R.B., M. Jordan, R. Steinberger, C. M. Puskas, J. Farrell, G. P. Waite, S. Husen, W.-L. Chang, and R. O'Connell (2009), Geodynamics of the Yellowstone hotspot and mantle plume: seismic and GPS imaging, kinematics, and mantle flow, *J. Volcanol. Geotherm. Res. 188*, 26–56.

Spada, G. (2001), Mantle viscosity from Monte Carlo inversion of very long baseline interferometry data, *J. Geophys. Res.*, *106*, 16,375–16,385.

Thatcher, W. (1983), Nonlinear strain buildup and the earthquake cycle on the San Andreas fault, *J. Geophys. Res.*, *88*, 5893–5902, 1983.

Thatcher, W., G. R. Foulger, B. R. Julian, J. Svarc, E. Quilty, and G. W. Bawden (1999), Present-day deformation across the Basin and Range province, western United States, *Science*, *283*,1714–1718.

Thatcher, W., and F. F. Pollitz (2008), Temporal evolution of continental lithospheric strength in actively deforming regions, *GSA Today*, *18*, 4–11.

Waite, G. P., and R. B. Smith (2002), Seismic evidence for fluid migration accompanying subsidence of the Yellowstone caldera, *J. Geophys. Res.*, *107*, doi:10.1029/2001JB000586.

Westaway, R., and R. B. Smith (1989), Source parameters of the Cache Valley (Logan), Utah, earthquake of 30 August 1962, *Bull. Seismol. Soc. Am. 79*, 1410–1425.

Williams, S. D. P., Y. Bock, P. Fang, P. Jamason, R. M. Nikolaidis, and L. Prawirodirdjo (2004), Error analysis of continuous GPS position time series, *J. Geophys. Res.*, *109*, B03412, doi:10.1029/2003JB002741.